Nanoscale

Accepted Manuscript

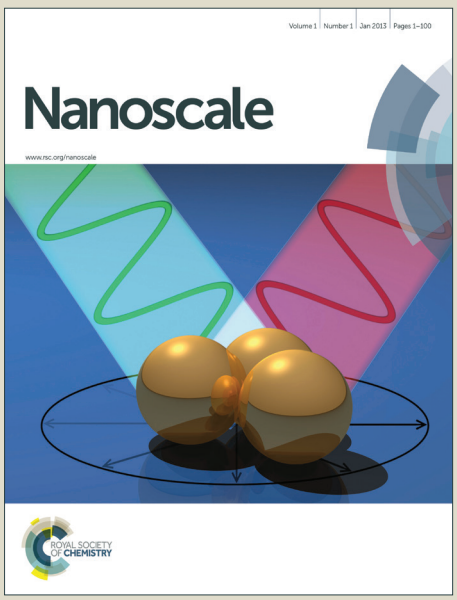

This is an *Accepted Manuscript*, which has been through the Royal Society of Chemistry peer review process and has been accepted for publication.

Accepted Manuscripts are published online shortly after acceptance, before technical editing, formatting and proof reading. Using this free service, authors can make their results available to the community, in citable form, before we publish the edited article. We will replace this *Accepted Manuscript* with the edited and formatted *Advance Article* as soon as it is available.

You can find more information about *Accepted Manuscripts* in the Information for Authors.

Please note that technical editing may introduce minor changes to the text and/or graphics, which may alter content. The journal's standard Terms & Conditions and the Ethical guidelines still apply. In no event shall the Royal Society of Chemistry be held responsible for any errors or omissions in this *Accepted Manuscript* or any consequences arising from the use of any information it contains.

ROYAL SOCIETY OF CHEMISTRY

www.rsc.org/nanoscale

Nanoscale

RSCPublishing

COMMUNICATION

Hydrothermal synthesis of Pt-Ag alloy nanooctahedra and their enhanced electrocatalytic activity for the methanol oxidation reaction†

Cite this: DOI: 10.1039/x0xx00000x

Geng-Tao Fu,‡[b] Ru-Guang Ma,‡[c] Xue-Qing Gao,[a] Yu Chen,*[ab] Ya-Wen Tang,[b] Tian-Hong Lu,[b] and Jong-Min Lee*[c]

Received 00th January 2012,
Accepted 00th January 2012

DOI: 10.1039/x0xx00000x

www.rsc.org/

The high-quality $Pt_{48}Ag_{52}$ alloy nanooctahedra are synthesized via one-pot hydrothermal method. The catalytic growth of Ag^0 atoms on Pt nuclei and selective oxidative etching on the Ag^0 atoms contribute to the formation of alloy nanooctahedra. $Pt_{48}Ag_{52}$ alloy nanooctahedra show excellent electrocatalytic activity and durability for the methanol oxidation reaction (MOR).

Octahedron, one of simplest Platonic solids, has 8 equilateral triangle faces, which is one end of the growth morphologies of Platonic solids.[1, 2] Recently, face-centered cubic (*fcc*) noble-metal nanooctahedra have found wide applications in catalysis, photonics, sensing, surface-enhanced Raman spectroscopy and fabrication of superstructures because of their interesting properties, such as high symmetry, the existence of critical edges, and complete {111} facets, *etc.*[3-10] At present, Pt-based bimetallic alloy nanocrystals have been widely used as an essential catalytic substance in various fields due to modified geometric and electronic structures of Pt.[11-15] For example, the spheric Pt-Ag alloy nanocrystals[14] and Pt-Ag alloy hollow nanoboxes[15] exhibited improved electrocatalytic activity for the methanol oxidation reaction (MOR) compared with Ag@Pt core-shell nanocrystals and Pt/C catalyst, respectively. To date, several Pt-Ag alloy nanocrystals with different morphologies, such as boxes, wires, sponges, flowers, and spheres, have been synthesized by various chemical reduction methods, including galvanic replacement and co-chemical reduction, *etc.*[16-20] Despite those impressive advances in synthesis, the shape-controlled synthesis of Pt-Ag alloy nanocrystals is still troubled by some issues, such as undefined reaction mechanism, complex reaction steps, low alloying degree, low yield/purity, and unsatisfactory uniformity.

In particular, so far, the synthesis of the Pt-Ag nanocrystals with high alloying degree is still very difficult because of three main reasons: (i) the different reduction kinetics of Pt^{n+} and Ag^+ precursors (*i.e.*, their distinct standard reduction potentials);[21, 22] (ii) the large lattice mismatch between Pt and Ag atoms (4.2%);[23] and (iii) the large miscibility gap between Pt and Ag in the bulk (*e.g.*, the Pt-Ag alloys could only form with the atomic composition of Ag:Pt<2:98 or Ag:Pt>95:5 at 400 °C).[19] Herein, we demonstrate a facile and energy-saving one-pot hydrothermal method to synthesize the $Pt_{48}Ag_{52}$ bimetallic nanocrystals with high alloying degree and well-defined nanooctahedral morphology. To the best of our knowledge, there is no report on the preparation of well-defined Pt-Ag alloy nanooctahedra. The as-prepared Pt-Ag alloy nanooctahedra exhibit remarkably improved electrocatalytic activity and durability for the MOR over commercially available Pt black.

In a typical synthesis, Pt-Ag alloy nanooctahedra were achieved by reducing K_2PtCl_4 and $AgNO_3$ precursors with HCHO in aqueous polyallylamine hydrochloride (PAH) solution at 180 °C for 4 h (see Experimental section for details). The energy dispersive X-ray (EDX) analysis indicates that the average composition of the products is $Pt_{48}Ag_{52}$ (Fig. S1, EIS†), which is similar to the $K_2PtCl_4/AgNO_3$ feeding ratio (50:50) in the initial reaction system. X-ray photoelectron spectroscopy (XPS) investigation shows the Ag^0 and Pt^0 species are dominant in the products (Fig. S2, EIS†), indicating the Pt^{II} and Ag^I precursors are completely reduced in our synthesis. Representative large-area transmission electron microscopy (TEM) image shows that the majority (>90%) of the Pt-Ag nanocrystals is regular nanooctahedra with an average edge length of 20±4.0 nm (Fig. 1A and insert). High-resolution TEM (HRTEM) image reveals that the surface of the Pt-Ag nanooctahedra is smooth with no obvious defects (Fig. 1B). The magnified HRTEM images clearly show the interval between the two lattice fringes is 0.2293 nm (Fig. 1C), smaller than that of the {111} lattice spacing of the *fcc* Ag crystal (0.2359 nm, JCPDS no. 04-0783) but larger than that of the *fcc* Pt crystal (0.2265 nm, JCPDS no. 04-0802), which is indicative of Pt-Ag alloy formation. The corresponding fast Fourier transform (FFT) patterns with irradiation along [110] zone axis demonstrate that the Pt-Ag nanooctahedra are single-crystalline with the {111} lattice facet as the basal surface (Fig. 1D). High-angle annular dark-field scanning TEM (HAADF-STEM) image confirms that the nanooctahedra are dominant

Nanoscale Accepted Manuscript

species in the products (Fig. 1E). The magnified HAADF-STEM image reveals the same luminance (Fig. 1F), indicating that the Pt-Ag nanooctahedra have an alloy structure rather than a core-shell structure.[24, 25] EDX elemental mapping pattern (Fig. 1G) and EDX line scanning profile (Fig. 1H) clearly show the distribution of Pt atoms is completely consistent with that of Ag atoms, confirming the alloy structure. X-ray powder diffraction (XRD) measurement shows that the Pt-Ag nanooctahedra can be identified as *fcc* structure (Fig. S3, EIS†). Using Vegard's law, the alloying Ag content in the Pt-Ag alloy nanooctahedra (with respect to Pt) is calculated to be 49 at.%, in consistent with the EDX composition (atomic ratio of Ag and Pt is 52:48), indicating that the Pt-Ag nanooctahedra are indeed an alloy structure rather than a mixture of monometallic and core-shell structure.

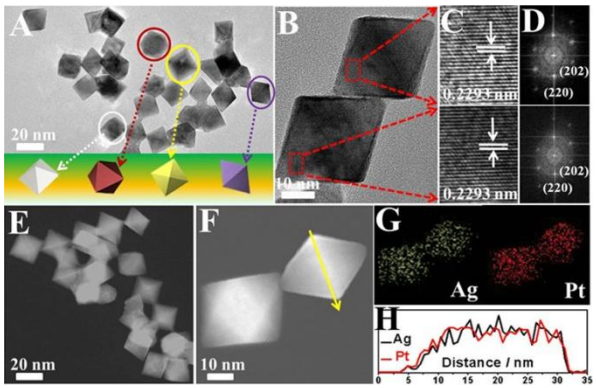

Fig. 1 (A) Typical TEM image of the Pt-Ag alloy nanooctahedra. The bottom insert is the four schematic drawings of an octahedron in four different orientations, which correspond to projected shapes of octahedron marked by circles. (B) HRTEM image of the Pt-Ag alloy nanooctahedra. (C) The magnified HRTEM image recorded from regions marked by squares in Figure B and (D) corresponding FFT patterns. (E) Typical HAADF-STEM image of the Pt-Ag alloy nanooctahedra. (F) The magnified HAADF-STEM image of the Pt-Ag alloy nanooctahedra and (G) the corresponding EDX elemental mapping patterns. (H) EDX line scanning profile of the Pt-Ag alloy nanooctahedra recorded from Figure F.

In our synthesis, PAH appears to be a vital component for the successful formation of the Pt-Ag alloy nanooctahedra. In the process of mixing precursors, PAH can provide Cl^- ion to generate white AgCl precipitate (Fig. S4, EIS†). In the absence of PAH, irregular and random-aggregation nanocrystals are obtained under the standard experimental conditions (Fig. S5, EIS†). This fact indicates that PAH with bulky molecule size and excellent hydrophilic property[26, 27] can serve as effective capping agent to ensure the dispersity of the Pt-Ag alloy nanooctahedra. Meanwhile, the interaction between PAH and K_2PtCl_4 results in the generation of the PAH-Pt^{II} complex,[26, 27] which decreases the reduction rate of the Pt^{II} species. Thus, in the absence of Ag^I, the monodisperse 10 nm Pt nanocubes with {100} facets are obtained by kinetically controlled synthesis (Fig. S6, EIS†). In turn, this fact demonstrates that the introduction of Ag^I species into the reaction system is critical to the octahedral morphology of the Pt-Ag alloy nanocrystals. Recently, Pd nanooctahedra were successfully prepared from Pd nanocubes in an HCl/O_2 aqueous solution based on oxidative etching and regrowth mechanism.[28] As mentioned above, 10 nm Pt nanocubes are obtained by the standard reaction procedure, indicating the formation of Pt-Ag alloy nanooctahedra can not be ascribed to the oxidative etching and regrowth of Pt nanocubes. In similar, Xiong observed that Ag nanocubes could evolve into Ag nanospheres due to oxidative etching.[29] Thus, we speculate that the oxidative etching of Ag^0 atoms on original intermediates may play a key role in determining the octahedral morphology of Pt-Ag nanocrystals. It is worth noting that the single-component Ag^I precursor (*i.e.*, AgCl precipitate) can not be reduced under the present experimental conditions, indicating that the reduction of Ag^I precursor is facilitated by the preformed Pt crystal nuclei through the catalytic growth mechanism.[30, 31] Based on these experimental observation and discussion, we infer that the formation of Pt-Ag alloy nanooctahedra mainly originates from the catalytic growth of Ag on Pt and selective oxidative etching of Ag^0 atoms, as shown in Scheme 1.

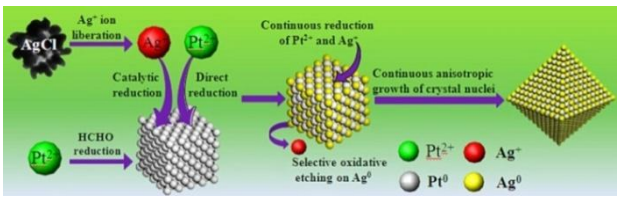

Scheme 1. Progressive formation of the Pt-Ag alloy nanooctahedra.

To better confirm the formation/growth process of the Pt-Ag alloy nanooctahedra, the intermediate nanocrystals produced at different reaction stages were investigated by TEM and EDX. At 30 min, the collected intermediates possess like-spheres morphology with sizes in the range of 200–300 nm (Fig. 2A). EDX analysis shows that the products consist of Ag and Cl elements with 1:1 atom ratio (Fig. S7A, EIS†), indicating that both Pt^{2+} (no Pt element is detected in products) and AgCl are not reduced by HCHO at 30 min. At 1 h, the content of Pt element increases to 4.35% (Fig. S7B, EIS†), Meanwhile, like-spheres AgCl nanocrystals evolve into porous AgCl nanocrystals (Fig. 2B and insert a-b), accompanying with small-size nanocrystals growth (Fig. 2B). The magnified TEM images (insert c) and EDX mapping patterns (insert d) show these small-size nanocrystals are the Pt-Ag alloy cuboctahedra. The previous report has demonstrated that Ag^+ ion can take place underpotential deposition (UPD) on the Pt surface,[32, 33] which decreases the Gibbs free energy of Ag^+ reduction. Thus, Ag^+ ions liberated from AgCl at high temperature can be reduced by HCHO and deposit preferentially on the Pt nuclei surface according to the thermodynamic viewpoint. Similar to the cases of Pd-Ni[30] and Pt-Ni[11] alloy nanocrystals, the deposited surface Ag atoms are then mixed with Pt atoms through an interdiffusion process, accompanying the simultaneously direct reduction of Pt^{II} precursor, and Pt-Ag alloy ultimately forms. At 2 h, EDX analysis shows that the intermediates consist of Pt and Ag elements with 58:42 atom ratios (Fig. S7C, EIS†). TEM image shows AgCl nanocrystals disappear completely and truncated Pt-Ag nanooctahedra are clearly observed in the products (Fig. 2C). As the reaction proceeded to 4 h, EDX analysis shows that Pt/Ag atom ratio is 52:48 (Fig. S7D, EIS†). And, TEM image shows the complete Pt-Ag alloy nanooctahedra generate (Fig. 2D).

The formation/growth process of the Pt-Ag octahedra was also reflected by XRD measurements. At 30 min, the strong AgCl diffraction peaks are observed (JCPDS no. 31-1238), and no Pt diffraction peaks are found (Fig. S8a, EIS†), further demonstrating the

Nanoscale Accepted Manuscript

This journal is © The Royal Society of Chemistry 2012

formation of AgCl nanocrystals at the initial stage. At 1 h, the diffraction peaks can be indexed as a mixture of AgCl nanocrystals and Pt-Ag nanocrystals (Fig. S8b, EIS†). When the reaction time further increases, the diffraction peaks of AgCl vanished and the strong diffraction peaks of Pt-Ag nanocrystals are observed (Fig. S8c-d, EIS†), indicating that complete Pt-Ag alloy nanocrystals generate at 2h and 4h.

In a controlled experiment without O_2, the irregular Pt-Ag nanocrystals are obtained by displacing the air with N_2 to eliminate typical etchant O_2 (Fig. S9, EIS†). Thus, it is safe to state that selective oxidative etching on Ag^0 atoms is critical in determining the octahedral morphology of the products. During the whole reaction, the Pt-Ag cuboctahedra, Pt-Ag truncated octahedra, and Pt-Ag octahedra are orderly observed at different reaction stages, which is typical characteristic of the evolution from nanocubes to nanooctahedra via the oxidative etching.[28, 34] In the course of the evolution, the active atoms from corners are selectively removed due to the oxidative etching by oxygen. Meanwhile, the strong adsorption of Ag^+ ion on Pt {100} facets and corresponding catalytic reduction of Ag^+ ion by Pt nuclei result in the continuous deposition of Ag on the Pt {100} facets.[35] The two factors ultimately lead to the formation of an octahedron enclosed by {111} facets.[29, 34] Additionally, the progressive increase in particle diameter of intermediates indicates that continuous atomic addition step should be involved in synthesis. Specifically, the continuous anisotropic growth of crystal nuclei (the continuous addition of Pt and Ag atoms reduced by HCHO on edges of intermediates), as well as periodic deposition and reoxidation of Ag atoms on the growing intermediates ultimately result in the formation of Pt-Ag alloy nanooctahedra.

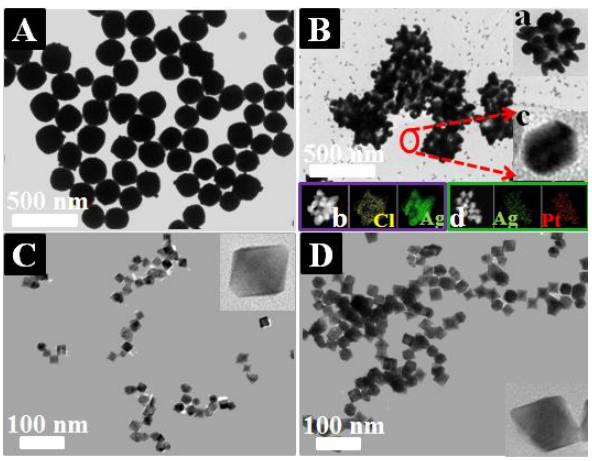

Fig. 2 TEM images of the intermediates collected at different growth stages: (A) 30 min, (B) 1 h, (C) 2 h, and (D) 4 h. Insert a and b in Figure B show the magnified TEM image and elemental mapping patterns of AgCl nanocrystals, respectively. Insert c and d in Figure B show the magnified TEM image and elemental mapping patterns of intermediates with small size, respectively.

The electrochemical property of the Pt-Ag alloy nanooctahedra was first investigated by cyclic voltammetry (CV) measurements (Fig. 3A). No electrochemical dissolution of Ag is found, indicating that alloying with Pt can greatly enhance the electrochemical stability of Ag. After an additional 50 CV cycles, the Pt/Ag atom ratio (49.52:50.48) in Pt-Ag nanooctahedra is close to their initial value (48.26:51.74) (Figure S10), further confirming the introduction of Pt enhance the electrochemical stability of Ag. The electrochemically active surface area (ECSA) was calculated by measuring the charge collected in the hydrogen adsorption-desorption region and assuming a value of 0.21 mC cm^{-2} for the adsorption of a hydrogen monolayer. The ECSA of the Pt-Ag alloy nanooctahedra (12.0 m^2 g^{-1}) is lower than that of the commercial Pt black (17.5 m^2 g^{-1}), which is most likely due to the large particle size ($d_{XRD\text{-}Pt\text{-}Ag\ nanooctahedra}$ = 22.0 nm *vs.* $d_{XRD\text{-}Pt\ black}$ = 8.5 nm).[36,37] The electrocatalytic activity of the Pt-Ag alloy nanooctahedra was examined by taking methanol as a model molecule. ECSA-normalized cyclic voltammograms show the oxidation peak potential of methanol on the Pt-Ag alloy nanooctahedra negatively shifts ca. 43 mV compared to that of the commercial Pt black (Fig. 3B). In the positive scan, the specific anodic peak current density of methanol on the Pt-Ag alloy nanooctahedra (2.96 mA cm^{-2}) is 3.02 times higher than that on the commercial Pt black (0.98 mA cm^{-2}). The lower oxidation peak potential and bigger oxidation peak current density suggest that the Pt-Ag alloy nanooctahedra exhibit significantly better electrocatalytic activity than the commercial Pt black. It is worth noting that specific activity (2.96 mA cm^{-2}) of the Pt-Ag alloy nanooctahedra for the MOR is competitively compared to existing Pt-based nanocrystals including Pt nanowires (0.84 mA cm_{Pt}^{-2}), Pt-Co nanocrystals (1.07 mA cm_{Pt}^{-2}), Pt-Fe nanocrystals (1.2 mA cm_{Pt}^{-2}), Pt-Cu nanocrystals (1.26 mA cm_{Pt}^{-2}), and Pt-Ni nanocrystals (1.34 mA cm_{Pt}^{-2}).[38] It is well known that the MOR on the Pt surface in acidic electrolytes is a structure sensitive reaction. The previous report has indicated that the Pt^{39} facets facilitate the methanol oxidation through the direct pathway and exhibit a good CO tolerance.[40-42] Thus, the complete {111} facets of the Pt-Ag alloy nanooctahedra contribute to an increase in the activity for the MOR. Of course, like other Pt-Ag alloy nanocrystals, alloying Pt with Ag is also a key factor for improved electrocatalytic activity of the Pt-Ag alloy nanooctahedra for the MOR due to the synergistic alloying effects, including electronic effect, geometric effect, and bifunctional mechanism, *etc.*[14, 43-45]

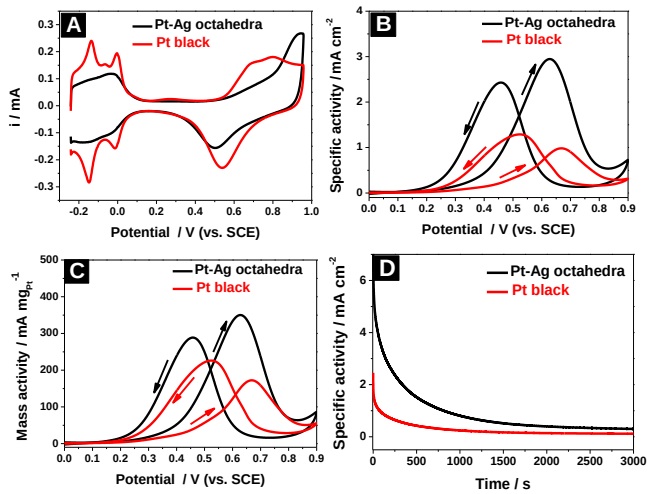

Fig. 3 (A) CV curves for the Pt-Ag alloy nanooctahedra and commercial Pt black in N_2-saturated 0.5 M H_2SO_4 solution at a scan rate of 50 mV s^{-1}. (B) ECSA-normalized and (C) Pt mass-normalized CV curves for the Pt-Ag alloy nanooctahedra and commercial Pt black in N_2-saturated 0.5 M H_2SO_4 + 1.0 M CH_3OH solution at a scan rate of 50 mV s^{-1}, respectively. Arrows indicate the

Nanoscale Accepted Manuscript

potential scan direction. (D) Chronoamperometry curves for the Pt-Ag alloy nanooctahedra and commercial Pt black in N_2-saturated 0.5 M H_2SO_4 + 1.0 M CH_3OH solution for 3000 s at 0.65 V potential.

The mass activity of electrocatalysts is generally used to assess the applicability of electrocatalysts. The mass-normalized cyclic voltammograms show the oxidation peak current of methanol on the Pt-Ag alloy nanooctahedra is 2.06 times higher than that on the commercial Pt black (Fig. 3C), indicating that Pt-Ag alloy nanooctahedra hold promise as potentially practical electrocatalysts for the MOR. The electrochemical stability of the Pt-Ag alloy nanooctahedra for the MOR were also investigated by chronoamperometric experiments (Fig. 3D). After 3000 s, the stable current density of the Pt-Ag alloy nanooctahedra is 0.72 mA cm^{-2}, which is about 4.8 times higher than that of Pt black (0.15 mA cm^{-2}). The above results indicate that the incorporation of Ag into Pt can enhance not only the electrocatalytic activity but also improve the electrocatalytic stability for the MOR in an acid media.

In summary, we successfully synthesized the $Pt_{48}Ag_{52}$ nanooctahedra with {111} facets and alloying structure via a facile one-pot hydrothermal route. The appearance of $Pt_{48}Ag_{52}$ alloy nanooctahedra indicates the phase diagram of bulk Pt-Ag alloy may not be applicable for the Pt-Ag bimetallic nanomaterials. During the reaction, Ag element from AgCl precipitate can transfer into the Pt-Ag alloy nanooctahedra due to the catalytic effect of a newly formed Pt intermediate for the Ag^+ reduction. The catalytic growth of Ag on the Pt intermediate and the interdiffusion between Ag and Pt atoms are responsible for the formation of the Pt-Ag alloy. The selective oxidative etching on Ag atoms and the continuous anisotropic growth of crystal nuclei play important roles in determining the octahedral morphology. Furthermore, the Pt-Ag alloy nanooctahedra displayed the remarkably improved electrocatalytic activity and stability for the MOR due to the facets effect and synergistic alloying effect. Thus, the Pt-Ag alloy nanooctahedra may be a promising anodic catalyst in direct methanol fuel cells and other advanced catalytic applications. Importantly, our synthesis reported here may offer a general approach to synthesize other Ag-noble metal (i.e., Pd, Ir, Au and Rh, etc.) alloy nanocrystals with controllable morphologies.

Acknowledgments

The authors are grateful for the financial support of NSFC (21376122 and 21273116), Natural Science Foundation of Jiangsu Province (BK20131395), United Fund of NSFC and Yunnan Province (U1137602), Industry-Academia Cooperation Innovation Fund Project of Jiangsu Province (BY2012001), Fundamental Research Funds for the Central Universities (GK201402016), Starting Funds of Shaanxi Normal University, Academic Research Fund of the Mistry of Education in Singapore (RGT27/13), and a project funded by the Priority Academic Program Development of Jiangsu Higher Education Institutions.

Notes and references

[a] *School of Materials Science and Engineering, Shaanxi Normal University, Xi'an 710062, PR China*
E-mail: ndchenyu@gmail.com (Y. Chen)

[b] *Jiangsu Key Laboratory of New Power Batteries, Jiangsu Collaborative Innovation Center of Biomedical Functional Materials, Analysis and Testing Center, School of Chemistry and Materials Science, Nanjing Normal University, Nanjing 210023, PR China*
[c] *School of Chemical and Biomedical Engineering Nanyang Technological University, Singapore 637459, Singapore*
E-mail: jmlee@ntu.edu.sg (J. M. Lee)

† Electronic Supplementary Information (ESI) available: Experimental and characterization data. See DOI: 10.1039/b000000x/
‡ Equal contribution to this work.

1. C. Li, K. L. Shuford, Q. Park, W. Cai, Y. Li, E. J. Lee and S. O. Cho, *Angew. Chem. Int. Edit.*, 2007, 119, 3328-3332.
2. J. Wu, A. Gross and H. Yang, *Nano Lett.*, 2011, 11, 798-802.
3. J. G. Zhang, Y. Gao, R. A. Alvarez-Puebla, J. M. Buriak and H. Fenniri, *Adv. Mater.*, 2006, 18, 3233-3237.
4. Y.-W. Lee, A.-R. Ko, D.-Y. Kim, S.-B. Han and K.-W. Park, *Rsc Adv.*, 2012, 2, 1119-1125.
5. M. Mulvihill, A. Tao, K. Benjauthrit, J. Arnold and P. Yang, *Angew. Chem. Int. Edit.*, 2008, 47, 6456-6460.
6. C. C. Li, K. L. Shuford, M. H. Chen, E. J. Lee and S. O. Cho, *ACS nano*, 2008, 2, 1760-1769.
7. S. I. Choi, S. F. Xie, M. H. Shao, J. H. Odell, N. Lu, H. C. Peng, L. Protsailo, S. Guerrero, J. H. Park, X. H. Xia, J. G. Wang, M. J. Kim and Y. N. Xia, *Nano Lett.*, 2013, 13, 3420-3425.
8. S. E. Habas, H. Lee, V. Radmilovic, G. A. Somorjai and P. Yang, *Nat. mater.*, 2007, 6, 692-697.
9. C.-C. Chang, H.-L. Wu, C.-H. Kuo and M. H. Huang, *Chem. mater.*, 2008, 20, 7570-7574.
10. Y.-W. Lee, A.-R. Ko, S.-B. Han, H.-S. Kim and K.-W. Park, *Phys. Chem. Chem. Phys.*, 2011, 13, 5569-5572.
11. Z. Niu, D. Wang, R. Yu, Q. Peng and Y. Li, *Chem. Sci.*, 2012, 3, 1925-1929.
12. X. Liu, G. Fu, Y. Chen, Y. Tang, P. She and T. Lu, *Chem. Eur. J.*, 2014, 20, 585-590.
13. J. Kugai, T. Moriya, S. Seino, T. Nakagawa, Y. Ohkubo, H. Nitani, K. Ueno and T. A. Yamamoto, *J. Phys. Chem. C*, 2013, 117, 5742-5751.
14. D. Zhao, B. Yan and B.-Q. Xu, *Electrochem. Commun.*, 2008, 10, 884-887.
15. W. Zhang, J. Yang and X. Lu, *ACS nano*, 2012, 6, 7397-7405.
16. J. Chen, B. Wiley, J. McLellan, Y. Xiong, Z.-Y. Li and Y. Xia, *Nano Lett.*, 2005, 5, 2058-2062.
17. Z. M. Peng, H. J. You and H. Yang, *ACS nano*, 2010, 4, 1501-1510.
18. C. L. Lee, Y. J. Chao, C. H. Chen, H. P. Chiou and C. C. Syu, *Int. J. Hydrogen Energ*, 2011, 36, 15045-15051.
19. Z. Peng and H. Yang, *J. Solid State Chem.*, 2008, 181, 1546-1551.
20. M. R. Kim, D. K. Lee and D. J. Jang, *Appl. Catal. B-Environ.*, 2011, 103, 253-260.
21. D. Zhao, Y.-H. Wang, B. Yan and B.-Q. Xu, *J. Phys. Chem. C*, 2009, 113, 1242-1250.
22. C. L. Li and Y. Yamauchi, *Phys. Chem. Chem. Phys.*, 2013, 15, 3490-3496.
23. W. He, X. Wu, J. Liu, X. Hu, K. Zhang, S. Hou, W. Zhou and S. Xie, *Chem. mater.*, 2010, 22, 2988-2994.
24. G. Fu, L. Ding, Y. Chen, J. Lin, Y. Tang and T. Lu, *CrystEngComm*, 2014, 16, 1606-1610.
25. G. Fu, K. Wu, J. Lin, Y. Tang, Y. Chen, Y. Zhou and T. Lu, *J. Phys. Chem. C*, 2013, 117, 9826-9834.

Nanoscale Accepted Manuscript

 This journal is © The Royal Society of Chemistry 2012

26. G. Fu, K. Wu, X. Jiang, L. Tao, Y. Chen, J. Lin, Y. Zhou, S. Wei, Y. Tang, T. Lu and X. Xia, *Phys. Chem. Chem. Phys.*, 2013, 15, 3793-3802.
27. G. Fu, R. Zhao, L. Ding, L. Tao, J. Lin, Y. Chen, Y. Tang, Y. Zhou and T. Lu, *ChemPlusChem*, 2013, 78, 623-627.
28. M. Liu, Y. Zheng, L. Zhang, L. Guo and Y. Xia, *J. Am. Chem. Soc.*, 2013, 135, 11752-11755.
29. Y. Xiong, *Chem. Commun.*, 2011, 47, 1580-1582.
30. K. Lee, S. W. Kang, S.-U. Lee, K.-H. Park, Y. W. Lee and S. W. Han, *Acs Appl. Mater. Interfaces*, 2012, 4, 4208-4214.
31. B. J. Hwang, Y. W. Tsai, L. S. Sarma, Y. L. Tseng, D. G. Liu and J. F. Lee, *J. Phys. Chem. B*, 2004, 108, 20427-20434.
32. E. Herrero, L. J. Buller and H. D. Abruna, *Chem. Rev.*, 2001, 101, 1897-1930.
33. S. A. Martínez, M. E. Martins and C. F. Zinola, *Electrocatal.*, 2011, 2, 172-180.
34. M. Jin, H. Zhang, Z. Xie and Y. Xia, *Energy Environ. Sci.*, 2012, 5, 6352-6357.
35. M. E. Grass, Y. Yue, S. E. Habas, R. M. Rioux, C. I. Teall, P. Yang and G. A. Somorjai, *J. Phys. Chem. C*, 2008, 112, 4797-4804.
36. J. Xu, G. Fu, Y. Tang, Y. Zhou, Y. Chen and T. Lu, *J. Mater. Chem.*, 2012, 22, 13585-13590.
37. G. Fu, X. Jiang, M. Gong, Y. Chen, Y. Tang, J. Lin and T. Lu, *Nanoscale*, 2014, 6, 8226-8234.
38. X. F. Yu, D. S. Wang, Q. Peng and Y. D. Li, *Chem. Eur. J.*, 2013, 19, 233-239.
39. C. A. Beasley, R. Sardar, N. M. Barnes and R. W. Murray, *J. Phys. Chem. C*, 2010, 114, 18384-18389.
40. T. H. M. Housmans, A. H. Wonders and M. T. M. Koper, *J. Phys. Chem. B*, 2006, 110, 10021-10031.
41. E. Herrero, K. Franaszczuk and A. Wieckowski, *J. Phys. Chem.*, 1994, 98, 5074-5083.
42. Y. G. Liu, Y. G. Wang, J. Y. Zhang, S. L. Shi, P. Feng and T. H. Wang, *Catal. Commun.*, 2009, 10, 1244-1247.
43. K. Kim, K. L. Kim and K. S. Shin, *J. Phys. Chem. C*, 2011, 115, 23374-23380.
44. W. He, X. Wu, J. Liu, K. Zhang, W. Chu, L. Feng, X. Hu, W. Zhou and S. Xie, *J. Phys. Chem. C*, 2009, 113, 10505-10510.
45. B. M. Concha and M. Chatenet, *Electrochim. Acta*, 2009, 54, 6130-6139.

Nanoscale Accepted Manuscript